JGR Atmospheres

Key Points:

- Between 2008 and 2016, the global radiative forcing due to SO_2 emissions from China and the rest of the world was approximately equal
- Radiative forcing from biomass burning emission changes offset warming over China, but increased it globally
- Changes in biomass burning emissions dominated the aerosol radiative forcing over the Arctic over this period

Supporting Information:

Supporting Information may be found in the online version of this article.

Correspondence to:

Y. Chen,
ee21yc@leeds.ac.uk

Author Contributions:

Data curation: Y. Chen
Formal analysis: Y. Chen
Funding acquisition: C. E. Scott, S. R. Arnold
Supervision: S. T. Turnock, C. E. Scott, S. R. Arnold
Visualization: Y. Chen
Writing – original draft: Y. Chen
Writing – review & editing: Y. Chen, S. T. Turnock, C. E. Scott, S. R. Arnold

Radiative Response to Large Decline in Anthropogenic Emissions From China Between 2008 and 2016 Is Modified by Simultaneous Biomass Burning Emission Changes

Y. Chen[1] , S. T. Turnock[2,3] , C. E. Scott[1] , and S. R. Arnold[1]

[1]School of Earth and Environment, Institute for Climate and Atmospheric Science (ICAS), University of Leeds, Leeds, UK, [2]Met Office Hadley Centre, Exeter, UK, [3]University of Leeds Met Office Strategic (LUMOS) Research Group, University of Leeds, Leeds, UK

Abstract The recent large reduction in anthropogenic aerosol emissions across China has improved China's air quality but has potential consequences for climate forcing. This sharp reduction in anthropogenic emissions has occurred against a background influenced by changing regional biomass burning emissions over a similar period of time. Here, we use the UK Earth System Model (UKESM) to estimate aerosol instantaneous radiative forcing (IRF) due to changes in emissions of aerosols and precursors from biomass burning and anthropogenic sources (separately and in combination) over 2008–2016, with a focus on China and regions downwind. We also separately quantify the IRF due to changes in anthropogenic aerosol emissions inside China (CHN) and the Rest Of the World (ROW). Reductions in Chinese anthropogenic emissions of BC, SO_2 and OC contributed -0.30 ± 0.01, $+1.00 \pm 0.04$, and $+0.05 \pm 0.01$ W m^{-2}, respectively to IRF over China, accounting for ~97% of the total local anthropogenic aerosol IRF. These emission changes contributed a remote regional IRF of 0.22 ± 0.04 W m^{-2} over the North Pacific Ocean. The reduction in SO_2 emissions from China contributed a global IRF of equal magnitude to that from SO_2 emissions from ROW (~0.08 W m^{-2}). Changes in global biomass burning emissions contributed 0.03 W m^{-2} (equivalent to over 20% of the magnitude of anthropogenic aerosol IRF), enhancing the global anthropogenic aerosol IRF, whereas they partly offset the anthropogenic IRF over China. Meanwhile, biomass burning emissions dominated the total IRF (around 98%) over the Arctic.

Plain Language Summary Aerosol emissions from human activities are known to affect both regional and global climate. In this study, we used an atmospheric model to assess how cleaner air, especially from reductions in anthropogenic aerosol emissions over China in recent years (2008–2016), has influenced Earth's radiative balance. We focused on key aerosol types, or their precursors, including black carbon (BC), sulfur dioxide (SO_2), and organic carbon (OC). Our results show that the reduction in sulfate aerosols had the largest warming effect both locally over China, and in remote ocean regions of the North Pacific. Globally, the climate impact due to changes in emissions of SO_2 from China was equal to that due to changes in SO_2 from the rest of the world between 2008 and 2016. Meanwhile, we found that the potential increase in global wildfires may be offsetting some of the warming effect over China coming from the local anthropogenic aerosol emission changes. The climate impact over the Arctic between 2008 and 2016 is dominated by the change in emissions of aerosols from wildfires. Our results here show how air pollution emissions can influence regional and global climate, and the importance of considering changes in both anthropogenic aerosol and wildfire emissions in estimating total radiative effects over a given period.

1. Introduction

Aerosols are a key component of short-term climate forcers (SLCFs), defined as radiatively active atmospheric constituents having atmospheric lifetimes shorter than two decades (Szopa et al., 2021). Despite their relatively short atmospheric lifetimes, SLCFs have important impacts on climate and air quality (Smith & Mizrahi, 2013). Aerosols can affect both regional and global climate directly by leading to temperature changes through the absorption or scattering of solar radiation (Shindell & Faluvegi, 2009), known as Aerosol-Radiation Interactions (ARI), and indirectly by modifying cloud properties, known as Aerosol-Cloud Interactions (ACI) (W. Chen & Xu, 2010; Liu & Matsui, 2021). The latest IPCC Assessment reports an estimated total aerosol effective radiative forcing (ERF) of -1.1 [-1.7 to -0.4] W m^{-2} between 1750 and 2019 with medium confidence (Forster et al., 2021).

In addition, aerosols are an important component of air pollution, with substantial health impacts associated with exposure to particulate matter with aerodynamic particle diameters less than 2.5 μm ($PM_{2.5}$) (Cohen et al., 2017). In the last decade the Chinese government enacted a series of anthropogenic emission control policies to alleviate the problems associated with air pollution episodes. The leading environmental governance policies in China are the Five-Year Plans (FYPs) (Young et al., 2015); environmental protection has become incorporated into FYPs, appears as a separate chapter in the 6th FYP (1981–1985), and has become more specific in subsequent FYPs (Jin et al., 2016). Policies have also been developed following extreme pollution events. In 2013, a severe haze affected ∼1.3 million km^2 and ∼800 million people across most cities in Central, Northern and Eastern China. Following this pollution event, the Chinese government issued the "Air Pollution Prevention and Control Action Plan (APPCAP)"(R. J. Huang et al., 2015), which led to a significant reduction in $PM_{2.5}$ concentrations (Silver et al., 2018, 2025; Yu et al., 2022) and associated premature mortality (J. Huang et al., 2018; Silver et al., 2020; Yue et al., 2020) between 2013 and 2017.

Biomass burning emissions are also an important source of aerosol, affected by human activities as well as by changes in climatic conditions (S. Archibald et al., 2009; Kelley et al., 2019), further impacting both air quality and the Earth's climate (Akagi et al., 2011; Voulgarakis et al., 2015). Satellite observations show that the global burned area by fires had declined by 25% between 1997 and 2013 (Andela et al., 2017), which were mainly due to deforestation, land use change (Schultz et al., 2008) and agricultural fires (Rangel & Vogl, 2019). Despite this decline in global burned area, fire activities have become more frequent and intense at high latitudes, for example, Russia between 1996 and 2018 (Kirillina et al., 2020), and the risk of fires is likely to further increase due to climate change (Baker, 2022; Wasserman & Mueller, 2023). This trend may lead to a higher frequency of extreme fire events in the future, especially in the high latitudes, with surface temperatures in the Arctic increasing at a rate two to three times the global average (Schacht et al., 2019), and recently thought to be even larger (Rantanen et al., 2022). Silver et al. (2024) identified an increase in $PM_{2.5}$ from wildfires at high latitudes in the past two decades, although the health impacts of emissions from Arctic nation wildfires have declined as the average latitude of wildfires in Siberia shifts northward.

Changes to aerosol emissions have affected the radiative balance of the Earth System (Forster et al., 2021; IPCC, 2013). Myhre et al. (2017) compared seven global models and highlighted that the changes in total anthropogenic aerosol forcing between 1750 and 2010 ranged between −0.58 and −0.02 W m^{-2}, with an ensemble mean of −0.27 W m^{-2} for global all-sky direct radiative forcing. Similarly, Bellouin et al. (2020) reported that changes in anthropogenic aerosol emissions have led to an increase in aerosol optical depth (AOD) of approximately 14%–29% between 2005 and 2015, compared to 1850 levels. The radiative forcing from anthropogenic aerosols offsets about one- fifth to one- half of the radiative forcing due to the increase in greenhouse gas concentrations. Quaas et al. (2022) estimated that the radiative forcing due to aerosols increased by 0.1–0.3 W m^{-2} between 2000 and 2019 (i.e., became less negative), accounting for up to 12% of the total climate forcing observed in 2019 relative to 1750, according to IPCC estimates. Turnock et al. (2016) used HadGEM3-UKCA to simulate that clean air actions in Europe have had significant climate impacts, due to reductions in aerosols, and warmed the regional surface temperature by approximately 0.45 ± 0.11°C from 1970 to 2010. Leibensperger et al. (2012) emphasized that the aerosol direct and indirect (with cloud) radiative forcing over US became less negative and caused a decrease in cooling effect by 0.8 and 1.0 W m^{-2}, respectively, from 1990 to 2010. The reduction in SO_2 (and thus secondary sulfate formation) emissions contribute to a weaker cooling effect. Studies also estimate the radiative forcing due to fire emissions; Tian et al. (2022) used the chemistry-climate-vegetation model ModelE2-YIBs to show that the aerosols emitted from fire caused an ERF of −0.565 ± 0.166 W m^{-2}. This magnitude is approximately one-fifth of the total anthropogenic ERF over the industrial era (1750–2019), which is estimated at +2.72 [1.96 to 3.48] Wm^{-2} (Forster et al., 2021).

Some studies have suggested that China's clean air actions may affect the radiative balance and regional climate. Dang and Liao (2019) found the reduction of aerosol emissions in eastern China between 2012 and 2017 resulted in a regional average aerosol direct radiative forcing of 1.18 W m^{-2}. Y. Zheng et al. (2020) reported the reduction in China's aerosol emissions from 2006 to 2017 produced a regional net ERF of 0.48 ± 0.11 W m^{-2} and contributed to a 0.12 ± 0.02°C near surface air temperature increase both over East Asia.

Anthropogenic aerosols emitted in China not only affect the local radiative forcing over China but can also influence climate in other regions by being transported over long distance and impacting the radiative balance in those regions. Sand et al. (2013) highlighted that increased BC from mid-latitudes has a greater impact on Arctic

Sea ice concentration and temperature than the increase in local Arctic BC concentration by modulating meridional energy transfer in the first couple of years in the 21st century. Quinn et al. (2007) and Sobhani et al. (2018) also confirmed the long-range transport of atmospheric particles from the mid-latitudes to the Arctic is the main contributor to the Arctic aerosol burden. Salzen et al. (2022) used five ESMs to evaluate the changes in Arctic climate due to SLCFs from 2015 to 2050 will be equivalent to the climate effect of carbon dioxide reductions, and the long-range transport from Asia will also have an impact on the Arctic climate, although the impact will be much smaller than the local SLCFs climate effect. Studies also evidenced that the reduction of aerosol emissions from China can reduce the amount of aerosol transported to the North Pacific Ocean (NPO) (Zhu et al., 2020) and exacerbate warming (H. Wang et al., 2024), through aerosol-cloud interactions (Li et al., 2019; Y. Wang et al., 2020).

In this study, we quantify the radiative forcing associated with changes in anthropogenic and biomass burning aerosol emissions between 2008 and 2016, a period of substantial anthropogenic aerosol reductions over China. Studies have confirmed that large reductions in aerosol emissions can affect climate (Hodnebrog et al., 2024), however, there are limited studies quantifying the radiative forcing from individual aerosol components, which is necessary to fully understand the radiative impacts of emission mitigation measures. We therefore simulate the anthropogenic aerosols IRF, split by its three main components or precursor—BC, SO_2, and OC emissions individually, isolating the distinct contributions of each species. We further differentiate the effects of anthropogenic aerosol component emission changes from both inside and outside China from 2008 to 2016 to quantify their relative roles in driving global and regional IRF. In addition, we quantify the contribution of a potential increase in global biomass burning emissions and assess whether these changes offset or enhance the IRF due to anthropogenic aerosol emission reductions over East Asia and in downwind regions. This study provides new insights into the radiative impacts of recent substantial anthropogenic aerosol emission reductions and offers a more comprehensive understanding of the component-specific and source-specific (anthropogenic and biomass burning) drivers of aerosol IRF between 2008 and 2016. Section 2 describes the emission data sets we used in this study, the description of UKESM1 and how we set up the model, while the findings are discussed in Sections 3–6, followed by the conclusion in Section 7.

2. Data and Methods

2.1. Data Sets

2.1.1. Anthropogenic Aerosol Emissions

Anthropogenic emissions are obtained from the ECLIPSE (Evaluating the Climate and Air Quality Impacts of Short-Lived Pollutants, v6b) inventory, created with the global GAINS (Greenhouse gas—Air pollution Interactions and Synergies) model at a resolution of $0.5° \times 0.5°$ (Amann et al., 2011; Stohl et al., 2015). Here we use version 6b of ECLIPSE, which includes several updates compared to previous versions, such as adding a new waste sector, revised international shipping, and gridding patterns updated for several sectors, including power plants, flaring, transport, industry (https://previous.iiasa.ac.at/web/home/research/researchPrograms/air/ECLIPSEv6b.html). We analyse the impacts of a rapid decrease in anthropogenic emissions over China following their peak in 2008, captured by the ECLIPSE v6b emissions between 2008 and 2016. We compared the ECLIPSE emissions with CEDS (Community Emissions Data System) data produced in 2021 (O'Rourke et al., 2021), which is the updated version of CEDS data used in the CMIP6 (Coupled Model Intercomparison Project Phase 6) experiments (Hoesly et al., 2018) at the same resolution as ECLIPSE. The original version of CEDS data used in CMIP6 included inaccurate anthropogenic aerosol emissions over Asia (Z. Wang et al., 2021).

To investigate emissions from China in this study, we analyse the region 18°–53°N, 73°–135°E during the period between 2008 and 2016. We compare the anthropogenic aerosol emissions in the ECLIPSE inventory with emissions from the CEDS inventory between 2008 to the end year (2014) of CEDS inventory (Table 1). The anthropogenic BC and OC emissions in ECLIPSE decrease by 0.28 and 0.72 Tg year^{-1} between 2008 and 2016, representing a percentage decline of 20% and 25%, respectively. The anthropogenic SO_2 emissions in ECLIPSE show a much sharper decrease of 17.53 Tg year^{-1}, corresponding to a percentage reduction of 54% over the same period. However, the anthropogenic aerosol emissions in CEDS inventory either show opposite trends (BC and OC) or no significant changes (SO_2). Trends of BC, SO_2 and OC emissions in ECLIPSE and CEDS inventories between 2008 and 2016 are shown in Figure S1 in Supporting Information S2. Notably, CEDS reports about a factor of two higher BC and OC emissions than ECLIPSE, which is largely attributable to differences in their

Table 1

Total Anthropogenic BC, SO₂, and OC Emissions (Units: Tg year⁻¹) Over China From ECLIPSE and CEDS in 2008 and 2016/2014, and Difference in Emissions Between 2008 and 2016/2014

	ECLIPSE			CEDS		
	2008	2016	Difference	2008	2014	Difference
BC	1.34	1.06	−0.28	2.19	2.52	+0.33
SO₂	32.30	14.77	−17.53	37.01	36.92	−0.09
OC	2.64	1.91	−0.73	4.26	5.09	+0.83

Note. Emissions from AWB in ECLIPSE are removed from the total anthropogenic BC, SO₂, and OC emission to keep the same sector sources as the emissions in CEDS.

estimates of energy sector emission controls in China and reliance on coarse energy statistics (Figure S2 in Supporting Information S2; Hoesly et al., 2018; Ikeda et al., 2022; Z. Wang et al., 2021).

2.1.2. Biomass Burning Emissions

We analyse monthly global biomass burning emissions from the Global Fire Emission Database (GFED, v4.1; https://www.globalfiredata.org/), which was also used in CMIP6 simulations, with a resolution of $0.25° \times 0.25°$. For our model simulations, these emissions are regridded to the model grid of $1.875° \times 1.25°$. This version of GFED provides emission data for multiple species (e.g., BC, OC, and various gas-phase pollutants) categorized by six specific biomass burning sources, and includes updates to better account for small fires (Randerson et al., 2018). Each chemical and aerosol precursor species has different monthly emission factors (EF), which are based on (Akagi et al., 2011). We classify these specific sources in GFED_v4.1 into two fire categories: forest fires (boreal forest fires; tropical forest fires; and temperate forest fires) and all other fires (agricultural waste burning; peat fires; and savanna, grassland and shrubland fires). To account for substantial interannual variability in fire emissions, we use 5-year average emissions centered on 2008 (2006–2010) and 2016 (2014–2018) to represent the start and end periods of the period of interest (Figure S3 in Supporting Information S2). This approach gives a better representation of changes in average fire behavior over the period, avoiding anomalies such as the unusually high fire emissions over Siberia in 2008 (Table 2), which are not representative of longer-term changes in fire emissions. We focus on fire emissions over Siberia due to its geographical proximity to China, and potentially important contribution to regional radiative effects over China and the North Pacific, where anthropogenic emission changes from China also affect the regional radiation balance (Dang & Liao, 2019).

2.1.3. Satellite Data

We compared our model simulated aerosol optical depth (AOD) with the level-3 MODIS (Moderate Resolution Imaging Spectroradiometer) gridded atmosphere monthly global AOD product—MOD08_M3 (https://doi.org/10.5067/MODIS/MYD08_M3.061) from Terra satellite platform (Platnick et al., 2017). We evaluate the model by comparing the MODIS AOD at 0.55 μm wavelength over land for 2008 with model simulated AOD at the same wavelength.

We compared our model simulated upward shortwave radiative flux at the top of atmosphere (TOA) with the satellite CERES (the Clouds and Earth's Radiant Energy System) EBAF (Energy Balances and Filled) Ed4.2.1 level 3b products (Kato et al., 2018; Loeb et al., 2018; Wielicki et al., 1996) in 2008.

2.2. Model Experiments

We use UKESM1, a fully coupled Earth System Model (ESM) (Petters & Kreidenweis, 2007; Sellar et al., 2019), which incorporates the atmosphere-ocean model HadGEM3-GC3.1 as its underlying physical climate model (Williams et al., 2018). Here, we use UKESM1 in an atmosphere-only configuration (using prescribed historical values for sea surface temperatures and sea ice concentrations) with a horizontal resolution of $1.875° \times 1.25°$ and 85 vertical levels from the surface to 85 km height. We repeated each simulation 15 times, using the same anthropogenic emissions with different meteorological years (2000–2014) to account for the impact of meteorological and natural (non-fire) emissions variability, and so that we can better isolate the impacts from anthropogenic or biomass burning emission changes. The 3-D meteorological fields were nudged at 6-hr intervals to the European Centre for Medium-Range Weather Forecasts (ECMWF) Reanalysis (ERA-5) (Hersbach

Table 2

Comparison of 5-Year Averaged and Single Year Biomass Burning Emissions (Units: Tg year⁻¹) Over Siberia in GFED

	2006–2010 averaged	2014–2018 averaged	Difference	2008	2016	Difference
BC	0.08	0.12	+0.04 (50%)	0.16	0.12	−0.04 (−25%)
OC	1.16	2.19	+1.03 (89%)	2.49	2.18	−0.31 (−12%)

Table 3
Model Experiments Conducted in This Study With Information on the Anthropogenic or Biomass Burning Emissions Used in Each Experiment

Experiment name	Anthropogenic aerosol (ECLIPSE)				Biomass burning (GFED)
	All	BC	SO_2	OC	
Base08	2008	2008	2008	2008	2008
CHNBC16	2008	2016_in	2008	2008	2008
CHNSO$_2$16	2008	2008	2016_in	2008	2008
CHNOC16	2008	2008	2008	2016_in	2008
ROWBC16	2008	2016_out	2008	2008	2008
ROWSO$_2$16	2008	2008	2016_out	2008	2008
ROWOC16	2008	2008	2008	2016_out	2008
ANTH08_BB06-10	2008	2008	2008	2008	2006–2010 averaged
ANTH08_BB14-18	2008	2008	2008	2008	2014–2018 averaged
ANTH16_BB14-18	2016	2016	2016	2016	2014–2018 averaged

Note. All: emission years for all aerosols and chemical species used in model experiments; BC: black carbon; SO_2: sulfur dioxide; OC: organic carbon. CHN: emissions in China; ROW: emissions from the Rest Of the World (not including China). ANTH: anthropogenic emissions; BB: biomass burning. We ran each simulation for 15 meteorological years (2000–2014).

et al., 2020) for the 15 meteorological years. The United Kingdom Chemistry and Aerosol (UKCA) scheme (O'Connor et al., 2014), is incorporated into UKESM1 for simulating changes in the composition of the atmosphere (A. T. Archibald et al., 2020). The modal aerosol scheme, Global Model of Aerosol Process (GLOMAP-model) (Mann et al., 2010) is used to simulate aerosol processes such as nucleation and coagulation. These dynamically varying aerosol properties are then used to calculate aerosol optical properties, which influence radiative fluxes by directly absorbing or scattering shortwave and longwave radiation. Natural aerosol are interactive in our UKESM1 simulation setup. Sea-salt emissions are calculated interactively using a wind-speed-dependent parameterization (Gong, 2003; Mulcahy et al., 2020). Mineral dust emissions are generated by an independent dust scheme (Bellouin et al., 2011), while biogenic emissions are produced by the interactive iBVOC scheme (Mulcahy et al., 2020; Pacifico et al., 2011, 2012). The simulation includes microphysical processes outlined by Mulcahy et al. (2020). UKESM1 calculates aerosol-cloud interactions (cloud albedo and cloud lifetime effects) only in warm liquid clouds and does not include impacts on ice phase clouds (Mulcahy et al., 2020). However, the configuration of UKESM1 used here has been found to underrepresent the hygroscopic properties of organic aerosols (Petters & Kreidenweis, 2007) and thus also their aerosol-cloud interactions. UKESM1 represents organic carbon (OC) as purely scattering and does not include absorption by brown carbon (O'Connor et al., 2021), therefore, brown Carbon warming is not represented in this study. However, this UKESM1 configuration adopts a relatively absorptive BC optical treatment, originally chosen to partly compensate for missing absorption by brown carbon (Walters et al., 2019), which is different from other models in CMIP6. Nitrate aerosol is not represented in UKESM1, therefore, in this paper, "anthropogenic aerosols" refer specifically to BC, sulfate and OC from anthropogenic sources. The calculation of aerosol instantaneous radiative forcing (IRF) in UKESM1 is diagnosed by the double-call radiation configuration (Bellouin et al., 2013; Turnock et al., 2015). The first call simulates the aerosol radiative effect, which includes both natural and anthropogenic aerosol effects; the second call simulates the aerosol-free atmosphere radiative transfer, which does not include the impact from aerosols. The radiative forcing calculations presented in this study represent the difference in radiative effects from changes in aerosol emissions between 2008 and 2016.

2.2.1. Idealized Experiments

Table 3 describes our 11 model experiments, designed to calculate the aerosol radiative effect from changes in anthropogenic aerosol (both single component and total; top), and biomass burning (bottom), emissions over the period 2008–2016. Since the agricultural waste burning (AWB) sector is included in both the ECLIPSE anthropogenic emissions and the GFED biomass burning emissions, we remove AWB emissions from our
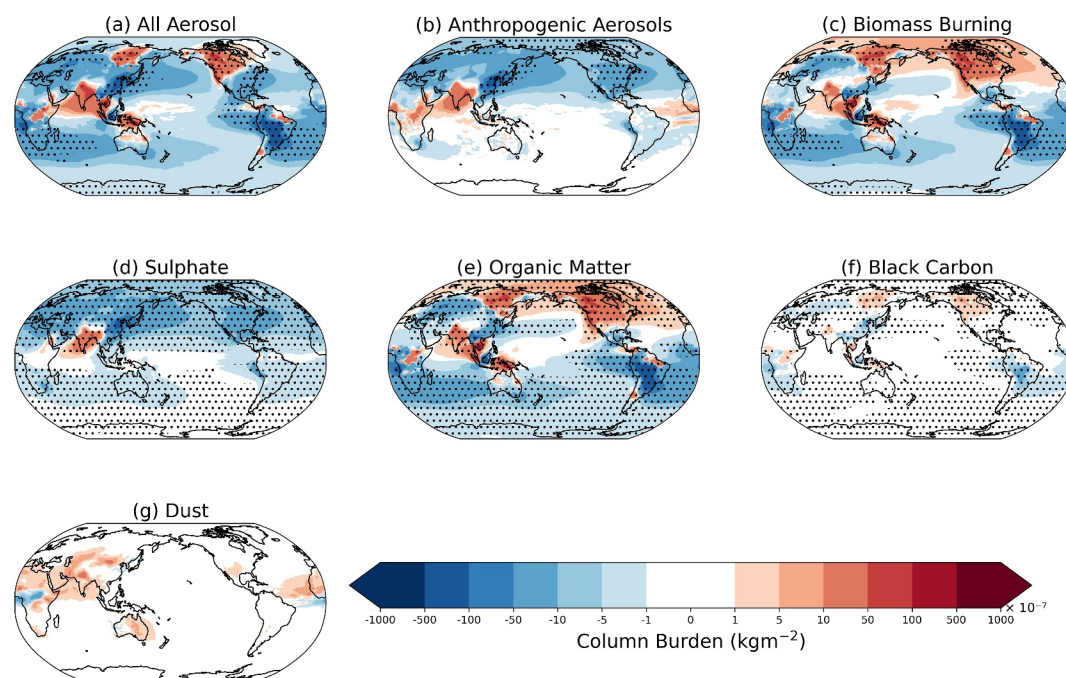
Figure 1. Changes in (a) total aerosols; (b) anthropogenic aerosols; (c) biomass burning; (d) sulfate; (e) organic matter; (f) black carbon; and (g) dust column burden between 2008 and 2016. The stippling denotes regions where the changes are significant ($p \leq 0.05$) based on a Student's t-test applied to the 15 years of model outputs.

anthropogenic ECLIPSE emissions and use these to replace the GFED AWB sector in the biomass burning emissions used in the anthropogenic perturbation experiments (BASE08, CHN*, and ROW*—see Table 3). In our 5-year mean biomass burning perturbation experiments (ANTH08_BB06-10; ANTH08_BB14-18; and ANTH16_BB14-18), GFED biomass burning emissions are used for all fire sectors (including AWB). We therefore use emission of all aerosols in 2008 (Base08) as the control experiment to explore the radiative forcing resulting from changes in aerosol species or the precursors, both inside and outside China, between 2008 and 2016. To examine the impact of only BC, SO_2, and OC emission changes across China, we individually replaced the emissions of BC, SO_2, and OC over China in Base08 with values for 2016 to obtain CHNBC16, CHNSO$_2$16, and CHNOC16, respectively. Similarly, we individually replace BC, SO_2, and OC emissions from the rest of the world with the values for 2016, and keep the emissions of all other species consistent with 2008 (i.e., the same as the emissions as in Base08) to obtain ROWBC16, ROWSO$_2$16, and ROWOC16, respectively. The radiative effect from individual anthropogenic aerosol species or precursors can be calculated by using the results from each experiment and subtracting the control model experiment (Base08).

We use three additional idealized experiments (Table 3) to diagnose the aerosol radiative effect from biomass burning emission changes. In experiments ANTH08_BB06-10 and ANTH08_BB14-18 respectively, we replace biomass burning emissions globally in Base08 with the values for the 5-year 2006–2010 average and 5-year 2014–2018 average biomass burning emissions (see Section 2.1.2). We use the anthropogenic aerosol emissions in 2016 from ECLIPSE and 5-year averaged biomass burning between 2014 and 2018 from GFED as the model input for ANTH16_BB14-18. The radiative forcing due to both anthropogenic aerosol and biomass burning emission changes can be calculated by using ANTH16_BB14-18 minus ANTH08_BB06-10. To isolate the radiative forcing from biomass burning emission changes, we can use the results from ANTH08_BB14-18 minus ANTH08_BB06-10. The radiative forcing from changes in global anthropogenic aerosols emissions change can be calculated using ANTH16_BB14-18 minus ANTH08_BB14-18.

3. Changes in Simulated Global Aerosol Column Burden Between 2008 and 2016

We analysed changes in the model-simulated aerosol column burden (Figure 1) between 2008 and 2016. The global total mass column burden of all aerosols (both anthropogenic aerosols and biomass burning emissions)

decreased by 0.62 Tg during this period, with 37% (−0.23 Tg) of reduction attributed to global anthropogenic aerosol (Figure 1b) and 63% (−0.39 Tg) to global biomass burning (Figure 1c). The biomass burning column burden changes were driven by OC, which accounted for 93% of the total biomass burning column burden change. Regionally, OC column burden increased over Southeast Asia, India, high latitudes in North Hemisphere (NH) and Africa but decreased elsewhere (Figure 1e).

UKESM1's baseline performance in simulating aerosol mass concentrations for the same model configuration has been evaluated by other studies. Mulcahy et al. (2020) demonstrated that UKESM1 reproduces key features of sulfate, BC, and OC, and provide an extensive evaluation of aerosol scheme within CMIP6 simulations. Hardacre et al. (2021) further compared UKESM1 with long term ground-based and satellite observations of SO_2, sulfate and dry deposition fluxes over Europe and the USA, which show that the model captures observed spatial and temporal patterns, though with some regional biases.

The reduction in anthropogenic aerosol column burden was dominated by changes in sulfate column burden (−0.27 Tg), as shown in Figure 1d, with offsets from other anthropogenic aerosol components. The changes in BC total column burden (Figure 1f) show similar changes to OC, but the magnitude is much smaller. The changes in dust column burden (Figure 1g) are not substantial.

Most regions experienced a reduction in aerosol column burden between 2008 and 2016, except for localized increases simulated over India, the northeastern part of Russia and high latitude Northern America. China had a large reduction in the column burden of all aerosols (8%), driven by a substantial decrease in sulfate, with a small contribution from reduction in OC and BC. This reduction was due to decreases in both anthropogenic aerosols and biomass burning emissions, with anthropogenic aerosol emission changes playing a dominant role (Figures 1a–1c). Similarly, the column burden over South America also decreased, which was primarily due to the reduction in biomass burning OC and BC emissions (Figures 1a and 1c).

The increase in aerosol column burden over India was caused by an increase of sulfate, OC and dust, while BC made negligible contributions between 2008 and 2016. The increase in aerosol column burdens over the northeastern part of Russia and the western United States were mainly caused by the biomass burning OC and BC emissions (Figures 1a and 1c), although this signal was partially offset by the reduction in sulfate column burden (Figure 1d).

4. Changes in Aerosol Optical Depth (AOD) Between 2008 and 2016

To evaluate our model simulations, we compared the UKESM1 simulated AOD in 2008 (Figure S4(a) in Supporting Information S2) with the AOD observed by the MODIS satellite in 2008 (Figure S4(b) in Supporting Information S2). Our model simulation captures the observed AOD pattern well in most regions, especially in the Northern Hemisphere. However, it underestimates the magnitude in some regions, particularly over dust source and outflow regions and over the Southern Ocean (Mulcahy et al., 2020). We analyse the changes in AOD from all aerosol emission changes between 2008 and 2016 (Figure 2a; ANTH16_BB14-18–ANTH08_BB06-10). We also use the various CHN and ROW simulations to attribute the regional AOD changes to different aerosol components. China had the largest reduction in AOD (Figure 2a), which is mainly a result of China's large reduction in SO_2 emissions (Figure 2e), as well as the reduction in China's BC (Figure 2d) and OC (Figure 2f) emissions during this time. Our findings are similar as the results presented by Filonchyk et al. (2019), who used MODIS and MISR data to analyse AOD trends across China from 2000 to 2017. Their study highlighted a notable reduction in AOD from both MODIS (24% decrease) and MISR (30% decrease) during their study period due to the environmental protection policy in China. AOD over the United States also showed a decline between the two time periods (Figure 2h). Our results are consistent with the results of Zhao et al. (2024) who used CAMS and highlighted that reduction in sulfate had a substantial impact on the declining trend of AOD over East China and Eastern United States between 2007 and 2019. However, AOD over South America, India, the South China Sea and its surrounding regions show increases, which were mainly caused by their local anthropogenic aerosol or precursor emission changes (Figures 2g–2i) between 2008 and 2016.
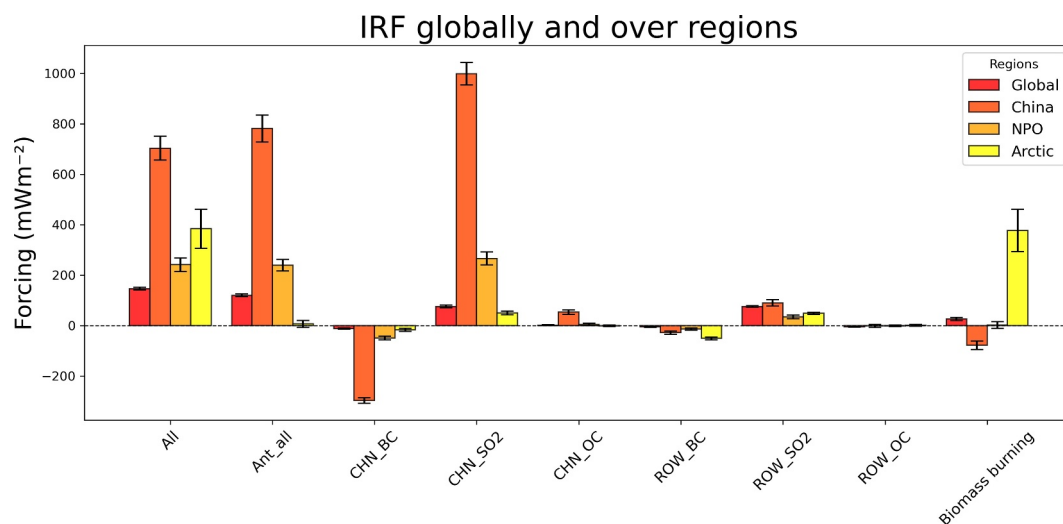
5. Aerosol Radiative Forcing Between 2008 and 2016

Changes in all aerosol emissions (anthropogenic and biomass burning) between 2008 and 2016 led to a positive radiative forcing across most regions of the world (Figures 3 and 4a, and Table S2 in Supporting Information S3),
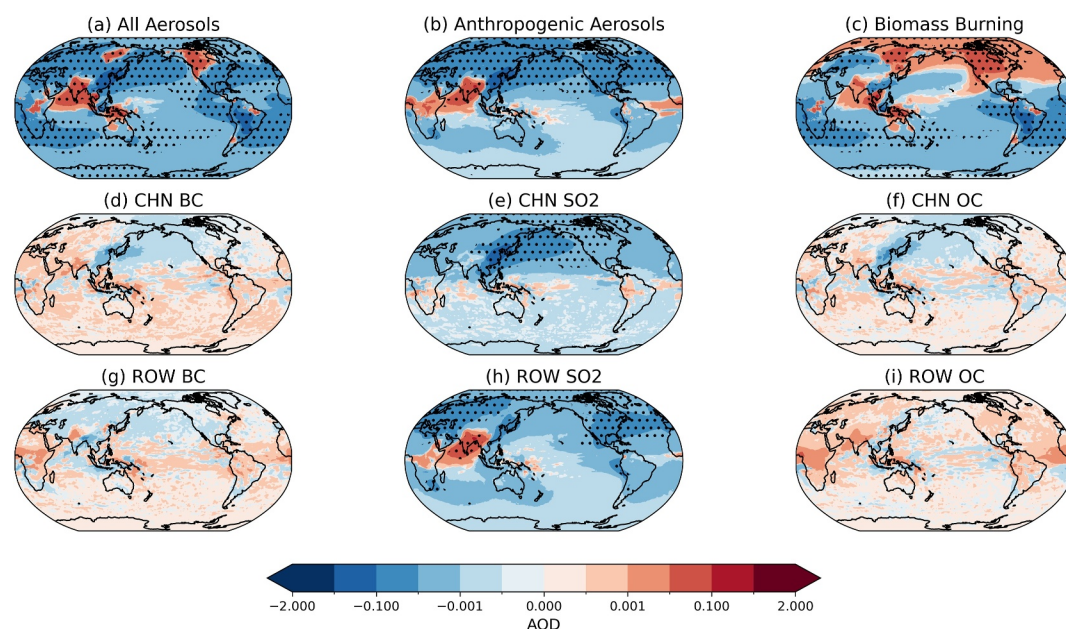
Figure 2. Changes in aerosol optical depth (AOD) from (a) all aerosols (anthropogenic + biomass burning); (b) anthropogenic aerosol only; (c) biomass burning only; and anthropogenic (d) BC; (e) SO_2; and (f) OC emissions inside China (CHN), and (g) BC; (h) SO_2; and (i) OC emissions from the rest of the world (ROW) between 2008 and 2016. The stippling denotes regions where the changes are significant ($p \leq 0.05$) based on a Student's t-test applied to the 15 years of model outputs.

with a positive global mean radiative forcing of 0.15 W m^{-2}, dominated by the large reduction in SO_2 emissions from China (17.53 Tg year^{-1}). This estimate is consistent with the latest RAMIP East Asia multi-model experiments (Wilcox et al., 2023), which simulates response to a comparable SO_2 reduction of ~20 Tg year^{-1} and reports global mean TOA effect radiative forcing values of 0.06–0.21 Wm^{-2} in response to the reduction of

Figure 3. Changes in the all-sky aerosol shortwave radiative forcing (units: mW m^{-2}) for model simulations between 2008 and 2016 globally, and over regions we focus on (Figure S6 in Supporting Information S2) China, North Pacific Ocean (NPO; 24°–45°N and 145°E–135°W); and the Arctic (60°–90°N). Positive (negative) values mean the radiative forcing increased (decreased). All: Anth16_BB14-18–Anth08_BB06-10; Anth_all: Anth16_BB06-10–Anth08_BB06-10; CHN_BC: CHNBC16–Base08; CHN_SO_2: CHNSO$_2$16–Base08; CHN_OC: CHNOC16–Base08; ROW_BC: ROWBC16–Base08; ROW_SO_2: ROWSO$_2$16–Base08; ROW_OC: ROWOC16–Base08; Biomass: Anth08_BB14-18–Anth08_BB06-10.
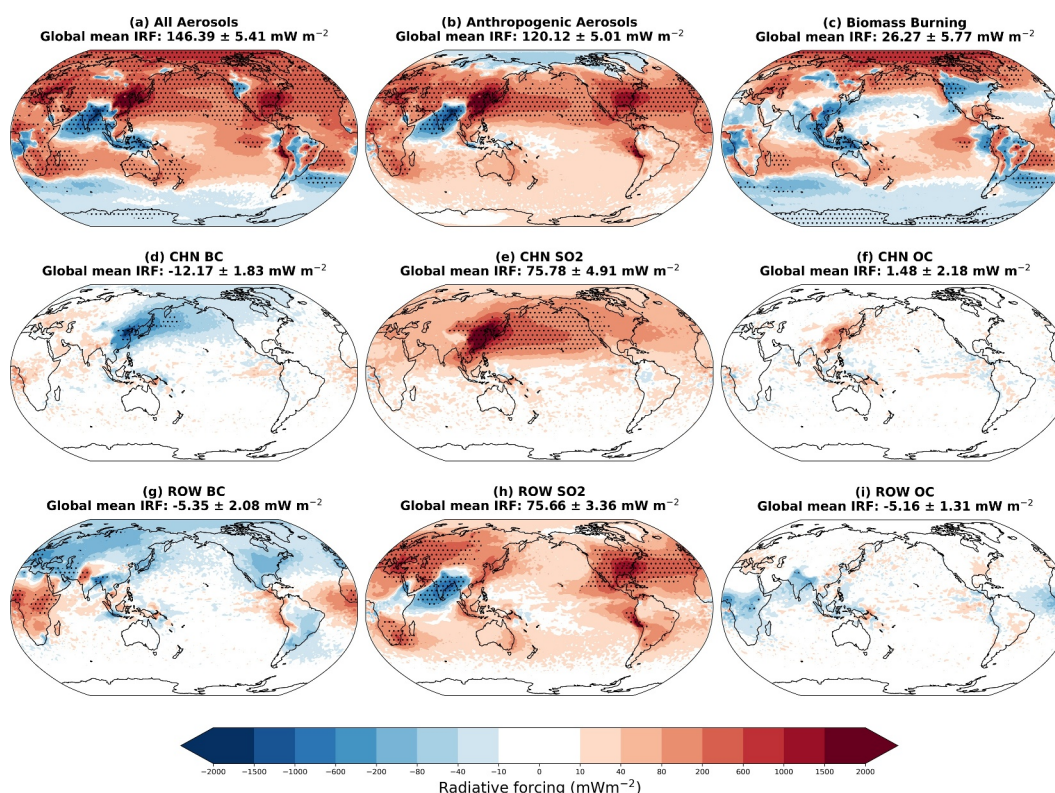
Figure 4. Changes in the all-sky aerosol radiative forcing due to changes in (a) global anthropogenic aerosol and biomass burning; (b) global anthropogenic aerosol; (c) global biomass burning; and inside China anthropogenic (d) BC; (e) SO_2 and (f) OC; and outside China anthropogenic (g) BC; (h) SO_2 and (i) OC emissions between 2008 and 2016. The stippling denotes regions where the changes are significant ($p \leq 0.05$) based on Student's t-test applied to the 15 years of model outputs.

anthropogenic aerosol emissions over East Asia, with sulfate aerosols dominating the forcing signal in the fixed-SST simulations (Samset et al., 2025). We evaluated our simulated upward shortwave radiative flux at TOA using the satellite CERES EBAF product to assess the performance of UKESM1 (Figure S5 in Supporting Information S2). This shows UKESM reproduces the large-scale spatial structure of upward SW radiation at TOA, with broadly similar magnitudes and modest regional differences. In our simulations, although the change in total column burden due to the reduction in biomass burning emissions (−0.38 Tg) is larger than the change in total column burden due to the reduction in anthropogenic aerosol (−0.23 Tg), anthropogenic aerosol emissions contributed the majority (−82%) of the total global aerosol radiative forcing, while biomass burning emission changes accounted for the remaining −18% (Figure 3).

In the northern hemisphere, the positive radiative forcing was primarily driven by the changes in anthropogenic aerosol emissions over low- and mid-latitude regions (Figure 4b). Meanwhile, the positive radiative forcing over the Arctic was mainly due to changes in biomass burning emissions (Figure 4c). However, this was partially offset by the radiative forcing from changes in anthropogenic aerosol emissions, with BC emission reductions from both CHN and ROW contributing to a negative forcing over the Arctic (Figure 4b). China had the largest positive aerosol regional radiative forcing (0.70 W m^{-2}, Figure 3), which was around five times larger than the global mean radiative forcing (0.15 W m^{-2}, Figure 3). By comparison, the regional aerosol-only radiative forcing over China calculated from CMIP6 experiments using CEDS emissions (see Text S1 in Supporting Information S1) was much larger with a negative value at −4.17 W m^{-2} between 2008 and 2014 from UKESM1 simulations. This pronounced difference highlights a substantial inconsistency in radiative forcing estimated using CEDS emissions data in CMIP6 historical experiments that fail to capture the sharp decline in China anthropogenic emissions over this recent time period (since 2008). The United States of America also has a significant positive radiative forcing signal due to changes in aerosol emissions between 2008 and 2016 (Figure 4). The positive aerosol radiative forcing over China and the USA were both mainly caused by the changes in anthropogenic aerosol emissions (Figure 4b), while the changes in biomass burning emissions offset some of this effect (Figure 4c). A negative

aerosol radiative forcing is simulated over India in Figure 4a, which was caused by increases in AOD (Figures 2e and 2f) from both sulfate and OC column burden (Figures 1b and 1c) between 2008 and 2016. The total radiative forcing over the Arctic due to changes in both global anthropogenic aerosols and biomass burning emissions is positive (0.38 W m, Figure 3), with changes in biomass burning emissions accounting for approximately 98% of aerosol radiative forcing changes in the region between 2008 and 2016. The 95% confidence levels (shown by the stippling) in Figure 4a indicate that the radiative forcing due to all (i.e., anthropogenic and biomass burning combined) aerosol emission changes is significant across much of the NH between 2008 and 2016. There are fewer locations in the Southern Hemisphere with a significant radiative forcing. There are significant forcing from much smaller anthropogenic emission changes in these regions compared with those in the midlatitudes of the Northern Hemisphere (Figures 4a and 4b).

5.1. Impacts of CHN Emission Changes

We analysed the radiative impact of changes in emissions from China only (Figures 4d–4f) over the period 2008 and 2016. Our results show a robust positive radiative forcing ($+1.00$ W m^{-2}) over China and NPO due to the recent rapid reduction in SO$_2$ emissions over China (Figures 3 and 4e). The aerosol radiative forcing due to the reduction in CHN SO$_2$ emissions only is centered mainly over Eastern China. Changes in sulfate resulting from CHN SO$_2$ emission changes also produce a significant remote radiative effect outside of the emission source region. The positive regional radiative forcing over NPO and the Arctic due to the reduction of CHN SO$_2$ emissions between 2008 and 2016 is 0.27 and 0.05 W m^{-2}, respectively (Figure 4e).

The reduction in BC emissions across China (Table 1) resulted in the presence of fewer aerosols that absorb solar radiation and therefore a reduced atmospheric heating effect. This change in BC emissions resulted in a slight negative global mean radiative forcing of -0.01 W m^{-2} and a much stronger negative radiative forcing of -0.3 W m^{-2} locally over China, with the highest aerosol radiative forcing centered in Eastern China, which is consistent with -0.33 W m^{-2} between 2008 and 2016 calculated by Liu and Matsui (2021). Changes in CHN BC emissions caused a much smaller forcing on the remote downwind North Pacific Ocean (NPO; -0.05 W m^{-2}) and the Arctic (-0.02 W m^{-2}) (Figure 3). Our result is slightly larger than the -0.033 W m^{-2} radiative forcing of BC over the Pacific obtained by Liu and Matsui (2021). It is worth noting that our radiative forcing from changes in CHN BC emissions show a poor degree of significance at the 95% confidence level outside Eastern China and the western part of NPO. This is primarily because the perturbation in CHN BC is relatively small, causing a weak IRF signal compared with the magnitude of the interannual variability.

We also analysed the radiative forcing caused by CHN OC emission changes between 2008 and 2016 (Figures 3 and 4f). In contrast with the radiative forcing from changes in CHN only BC and SO$_2$ emissions, the radiative forcing response to CHN OC emission changes is relatively small over China (0.05 W m^{-2}). We found no strong radiative forcing responses globally (0.001 W m^{-2}), or remotely over NPO (0.004 W m^{-2}) and the Arctic (-0.001 W m^{-2}) in response to changes to OC emissions from China. Our result shows the same poor degree of significance at the 95% confidence level globally. However, we attach more uncertainty to this result, given potential underestimation in hygroscopicity of OC in UKESM1 (see Section 2.2).

Our results suggest that aerosol radiative forcing due to the reduction in CHN BC, SO$_2$, and OC emissions between 2008 and 2016 account for approximately 97% of China's regional radiative forcing due to changes in all anthropogenic aerosol emission changes during this time period. The total radiative forcing from changes in CHN BC, SO$_2$, and OC emissions over NPO (0.22 W m^{-2}, Figure 3) is only slightly lower than the radiative forcing due to all aerosol changes (0.24 W m^{-2}), indicating that the anthropogenic aerosol radiative forcing over NPO is heavily dominated by the changes in aerosols emitted from China over this period, however, there are other aerosols that have an impact on the radiative forcing over NPO (discussed below). The results over the Arctic suggest a more complex response and influences from other source regions. The radiative forcing from changes in all global sources of anthropogenic aerosols in the Arctic is 0.01 W m^{-2}, while the total radiative effect due to changes in CHN BC, SO$_2$, and OC emissions (0.03 W m^{-2}) is about three times higher than that value. This result highlights the aerosol radiative forcing in the Arctic due to China emission changes was mostly offset by aerosol emission changes from elsewhere during this period (discussed below). Despite the substantial magnitude of China's SO$_2$ emission reduction between 2008 and 2016 (17.5 Tg), the resulting Arctic radiative response was much smaller than that associated with a comparable SO$_2$ emission reduction (around 17 Tg) from Europe between 1980 and 2005, which produced a net annual mean energy increase of 0.30 Wm^{-2} over the Arctic (Navarro

et al., 2016). This large difference in radiative response may reflect less efficient aerosol transport from East Asia to the Arctic compared with that from Europe (Stjern et al., 2019).

Studies suggest that China anthropogenic aerosol emissions continued to decline until 2019. The MEIC (Multi-resolution Emissions Inventory for China) shows that China's $PM_{2.5}$ and SO_2 emissions in 2017 were 35% and 62% lower, respectively, than in 2010 (B. Zheng et al., 2018), of the same magnitude as SO_2 emission reduction from China in our simulations. MEIC has since been extended to 2018 and 2019, confirming continued declines in these years (B. Zheng et al., 2021). The continued post-2016 decline in anthropogenic aerosol emissions from China would likely produce further negative global and regional IRF.

5.2. Impacts of Emission Changes From ROW

We also quantified the aerosol radiative forcing from changes in individual aerosol precursor emissions from ROW between 2008 and 2016 (Figures 3 and 4g–4i). Global radiative forcings from changes in ROW SO_2 emissions and CHN SO_2 emissions were approximately equal (0.08 W m^{-2}) over this period (Figure 3). Changes in ROW BC and OC emissions, however, produce much smaller global mean radiative forcing. Similar to the changes in radiative forcing due to changes in CHN aerosol emissions discussed above, the reduction in BC emissions from ROW caused a negative radiative forcing over China (−0.03 W m^{-2}). Conversely, the reduction in SO_2 emissions from ROW led to a positive radiative forcing over China (0.09 W m^{-2}). However, the impact of changes to ROW BC, SO_2, and OC emissions on the radiative forcing within China is relatively small (0.02 W m^{-2}), accounting for only about 10% of the total forcing over China. Although individual changes in emissions of ROW anthropogenic aerosol species (BC, SO_2 and OC) contribute to radiative forcing over the Arctic, the combined effect of these species (i.e., the sum of the radiative forcing due to changes in ROW BC, SO_2, and OC emissions) does not result in a significant overall radiative forcing over the Arctic.

5.3. Impacts of Changes in Biomass Burning Emissions

The global mean aerosol radiative forcing from changes in global biomass burning emissions between 2006–2010 and 2014–2018 (Figure 4c) was 0.03 W m^{-2} (Figure 3), accounting for 18% of the total aerosol radiative forcing between 2008 and 2016. The changes in biomass burning emissions led to a negative radiative forcing of −0.08 W m^{-2} over China, with a more substantial impact spatially concentrated in the northern parts of China. This negative RF partially offsets the positive radiative forcing from changes in anthropogenic aerosol emissions from both CHN and ROW. Meanwhile, changes in global biomass burning emissions during the period had negligible impact on the RF over NPO. In the Arctic, the radiative forcing from changes in biomass burning emissions (0.38 W m^{-2}, Figure 3) between the two time periods dominated (98%) the total aerosol radiative forcing over the Arctic caused by both anthropogenic aerosol and biomass burning emission changes.

6. Changes in Cloud Radiative Forcing Between 2008 and 2016

In addition to aerosol IRF, we also analysed the cloud radiative forcing (CRF) due to changes in both anthropogenic and biomass burning emissions between 2008 and 2016 (Figure 5, Figure S7 in Supporting Information S2 and Table S1 in Supporting Information S3). The global mean CRF from changes in all aerosol emissions between 2008 and 2016 is 0.17 ± 0.03 W m^{-2}. However, we find that the calculated change in CRF is not statistically significant ($p \le 0.1$), at any location. The CRF in most regions of the NH is positive, however, the CRF signal across the Southern Hemisphere (SH) is inconsistent and generally small as there are smaller anthropogenic aerosol emission changes in the SH. Overall, the CRF across China caused by changes in both anthropogenic aerosols and biomass burning emissions is positive (0.11 ± 0.06 W m^{-2}) from 2008 to 2016. However, the spatial pattern in CRF across China is more complex and is different from the large-scale positive aerosol instantaneous direct radiative forcing responses (discussed in Section 5). The CRF over China is approximately 16% of the magnitude of the IRF over China, suggesting that the direct aerosol radiative forcing dominates locally. There is a strong negative CRF signal over the Beijing-Tianjin-Hebei (BTH) region, while the signal of CRF over southeast China is positive (Figure 5). The strong negative CRF over BTH is due to the reduction in BC which weakens the semi-direct heating through cloud aadjustment, leading to more low cloud and a more negative CRF (Johnson et al., 2019), despite concurrent sulfate reduction. These patterns align with evidence that absorbing aerosols drive rapid circulation and precipitation adjustments (Johnson & Haywood, 2023; Johnson et al., 2019). Fang et al. (2023) also demonstrate that Asian monsoon rainfall is sensitive
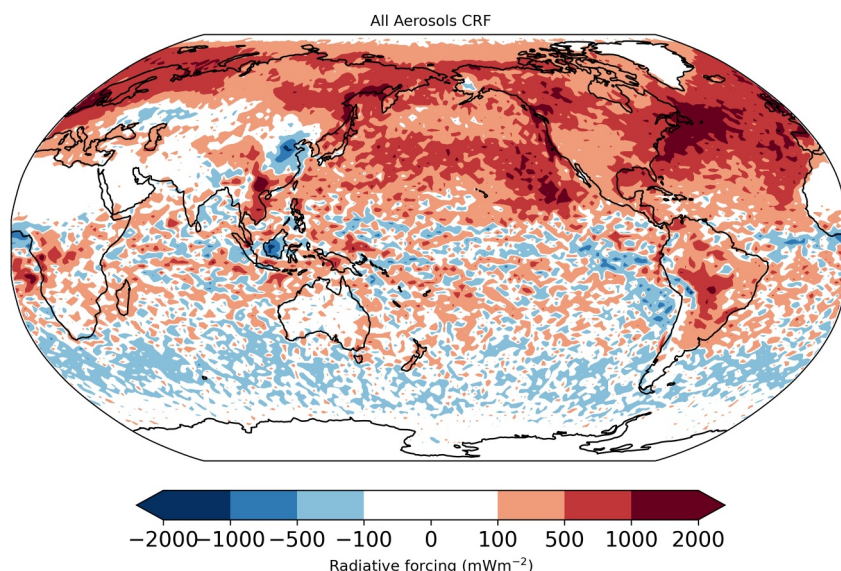
Figure 5. Cloud radiative forcing (units: mWm^{-2}) due to changes in both anthropogenic and biomass burning emissions between 2008 and 2016.

to the balance of scattering and absorbing aerosol reductions. No strong CRF response is found due to global biomass burning emission changes (Figure S7(b) in Supporting Information S2) between 2008 and 2016. The CRF over downwind NPO is positive and much larger than CRF response over China, which is 0.51 ± 0.07 W m^{-2}. The CRF response over NPO is dominated by the changes in anthropogenic emissions (0.58 ± 0.04 W m^{-2}), while biomass burning emission changes (-0.07 ± 0.05 W m^{-2}) partially offset the NPO CRF between 2008 and 2016. The magnitude of the CRF over the NPO is more than twice that of the IRF over NPO, suggesting that remote responses to emission reductions are mainly driven by impacts on clouds. The CRF over the Arctic (0.47 ± 0.06 W m^{-2}) is also positive and dominated by changes in anthropogenic emissions (0.52 ± 0.04 W m^{-2}), while the overall CRFs are negative from changes in biomass burning emissions (-0.06 ± 0.03 W m^{-2}) over the Arctic, especially over east Russia and Alaska.

7. Conclusions

We have isolated the local and remote radiative forcing due to changes in BC, SO_2, and OC emissions from both inside and outside China between 2008 and 2016. We have also estimated the radiative forcing from mean changes in biomass burning emissions over the same period, and shown important combined and offsetting influences from these emission changes in China and downwind regions.

We estimate a global annual mean aerosol radiative forcing of 0.15 W m^{-2} due to changes in both anthropogenic and biomass burning emissions between 2008 and 2016, and a regional forcing over China of 0.70 W m^{-2}. Our results show that the radiative forcing from changes to BC (-0.30 W m^{-2}), sulfate (1.00 W m^{-2}), and OC (0.05 W m^{-2}) averaged over China are mainly due to changes in local emission sources, with little influence from emission changes outside of China. Changes in SO_2 emissions from China and from the rest of the world have produced positive global radiative forcing values of equal magnitude (0.08 W m^{-2}) between 2008 and 2016. Changes in anthropogenic aerosol emissions outside of China account for only 10% of the total radiative forcing due to all anthropogenic aerosol emissions changes over China. Biomass burning emission changes have partially offset the radiative forcing due to anthropogenic aerosol emission changes over China, while enhancing anthropogenic forcing globally. In contrast with forcing from anthropogenic aerosol, biomass burning emissions have dominated IRF (~98%) over the Arctic between 2008 and 2016, likely due to substantial changes in biomass burning emissions from northern Eurasia. The Arctic has seen only small radiative impacts due to anthropogenic emission changes over this period (~2%), with some offsetting between impacts from SO_2 and BC emission changes. Aerosol emission reductions in China dominated the radiative forcing over NPO, while changes in anthropogenic aerosol emissions from China had no significant impacts on the Arctic radiative forcing between 2008 and 2016.

The changes in CRF over China between 2008 and 2016 vary across different regions and are primarily driven by changes in anthropogenic aerosol emissions. Specifically, a positive CRF signal is simulated over East China, while the CRF over the Beijing-Tianjin-Hebei region is negative. Changes in anthropogenic emissions dominated the CRF over NPO during these years. Although the direct aerosol radiative forcing over the Arctic is dominated by changes in biomass burning emission between 2008 and 2016, the CRF signal due to changes in anthropogenic emissions over Arctic is also large in magnitude (0.52 W m^{-2}), although of a low statistical significance.

Air quality in China has improved substantially in recent years due to a series of emission reduction measures. However, the reduction in anthropogenic aerosol emissions over China has resulted in a positive radiative forcing of equal size to emission changes from the rest of the world, and contributed to local and regional climate warming. Our global simulations indicate that over polluted Asian regions (China and India), local aerosol emission changes dominate the radiative forcing, but the changes are also important for long-range transport to remote regions, for example, Arctic and NPO. Between 2008 and 2016, as anthropogenic aerosol emissions reduced, emissions from biomass burning have shown an increasing trend in Eastern Eurasia, which has also been important for radiative forcing. This trend may become more important in the future if anthropogenic aerosol emissions continue to decrease, and biomass burning emissions increase due to climate change. Our results support the idea that air quality and climate policies need to be formulated in a co-ordinated manner and their impacts comprehensively evaluated.

Conflict of Interest

The authors declare no conflicts of interest relevant to this study.

Data Availability Statement

The ECLIPSE data used in this study are publicly available at https://iiasa.ac.at/models-tools-data/global-emission-fields-of-air-pollutants-and-ghgs (IIASA, 2019). CEDS data are publicly available at https://zenodo.org/records/3606753 (Hoesly et al., 2020). GFED data are publicly available at https://daac.ornl.gov/cgi-bin/dsviewer.pl?ds_id=1293. MODIS AOD data are publicly available at https://ladsweb.modaps.eosdis.nasa.gov/missions-and-measurements/products/MOD08_M3. Simulation NETCDF4 output files from UKESM1 for this paper is provided on Zenodo: https://zenodo.org/records/15611337 (Y. Chen et al., 2025).

References

Akagi, S. K., Yokelson, R. J., Wiedinmyer, C., Alvarado, M. J., Reid, J. S., Karl, T., et al. (2011). Emission factors for open and domestic biomass burning for use in atmospheric models. *Atmospheric Chemistry and Physics*, *11*(9), 4039–4072. https://doi.org/10.5194/acp-11-4039-2011

Amann, M., Bertok, I., Borken-Kleefeld, J., Cofala, J., Heyes, C., Höglund-Isaksson, L., et al. (2011). Cost-effective control of air quality and greenhouse gases in Europe: Modeling and policy applications. *Environmental Modelling & Software*, *26*(12), 1489–1501. https://doi.org/10.1016/j.envsoft.2011.07.012

Andela, N., Morton, D. C., Giglio, L., Chen, Y., Van Der Werf, G. R., Kasibhatla, P. S., et al. (2017). A human-driven decline in global burned area. *Science*, *356*(6345), 1356–1362. https://doi.org/10.1126/science.aal4108

Archibald, A. T., M O'Connor, F., Luke Abraham, N., Archer-Nicholls, S., P Chipperfield, M., Dalvi, M., et al. (2020). Description and evaluation of the UKCA stratosphere-troposphere chemistry scheme (StratTrop vn 1.0) implemented in UKESM1. *Geoscientific Model Development*, *13*(3), 1223–1266. https://doi.org/10.5194/gmd-13-1223-2020

Archibald, S., Roy, D. P., van Wilgen, B. W., & Scholes, R. J. (2009). What limits fire? An examination of drivers of burnt area in Southern Africa. *Global Change Biology*, *15*(3), 613–630. https://doi.org/10.1111/j.1365-2486.2008.01754.x

Baker, S. J. (2022). Fossil evidence that increased wildfire activity occurs in tandem with periods of global warming in Earth's past. *Earth-Science Reviews*, *224*, 103871. Elsevier B.V. https://doi.org/10.1016/j.earscirev.2021.103871

Bellouin, N., Mann, G. W., Woodhouse, M. T., Johnson, C., Carslaw, K. S., & Dalvi, M. (2013). Impact of the modal aerosol scheme GLOMAP-mode on aerosol forcing in the Hadley Centre global environmental model. *Atmospheric Chemistry and Physics*, *13*(6), 3027–3044. https://doi.org/10.5194/acp-13-3027-2013

Bellouin, N., Quaas, J., Gryspeerdt, E., Kinne, S., Stier, P., Watson-Parris, D., et al. (2020). Bounding global aerosol radiative forcing of climate change. *Reviews of Geophysics*, *58*(1), e2019RG000660. Blackwell Publishing Ltd. https://doi.org/10.1029/2019RG000660

Bellouin, N., Rae, J., Jones, A., Johnson, C., Haywood, J., & Boucher, O. (2011). Aerosol forcing in the climate model intercomparison project (CMIP5) simulations by HadGEM2-ES and the role of ammonium nitrate. *Journal of Geophysical Research*, *116*(20), D20206. https://doi.org/10.1029/2011JD016074

Chen, W., & Xu, R. (2010). Clean coal technology development in China. *Energy Policy*, *38*(5), 2123–2130. https://doi.org/10.1016/j.enpol.2009.06.003

Chen, Y., Turnock, S., Scott, C., & Arnold, S. (2025). UKESM1 TOA radiative fluxes due to changes in anthropogenic aerosol and biomass burning emissions [Dataset]. *Zenodo*. https://doi.org/10.5281/zenodo.15611337

Cohen, A. J., Brauer, M., Burnett, R., Anderson, H. R., Frostad, J., Estep, K., et al. (2017). Estimates and 25-year trends of the global burden of disease attributable to ambient air pollution: An analysis of data from the Global Burden of Diseases Study 2015. *The Lancet*, *389*(10082), 1907–1918. https://doi.org/10.1016/S0140-6736(17)30505-6

Dang, R., & Liao, H. (2019). Radiative forcing and health impact of aerosols and ozone in China as the consequence of clean air actions over 2012–2017. *Geophysical Research Letters*, *46*(21), 12511–12519. https://doi.org/10.1029/2019GL084605

Fang, C., Haywood, J. M., Liang, J., Johnson, B. T., Chen, Y., & Zhu, B. (2023). Impacts of reducing scattering and absorbing aerosols on the temporal extent and intensity of South Asian summer monsoon and East Asian summer monsoon. *Atmospheric Chemistry and Physics*, *23*(14), 8341–8368. https://doi.org/10.5194/acp-23-8341-2023

Filonchyk, M., Yan, H., Zhang, Z., Yang, S., Li, W., & Li, Y. (2019). Combined use of satellite and surface observations to study aerosol optical depth in different regions of China. *Scientific Reports*, *9*(1), 6174. https://doi.org/10.1038/s41598-019-42466-6

Forster, P., Alterskjaer, K., Smith, C., Colman, R., Damon Matthews, H., Ramaswamy, V., et al. (2021). The Earth's energy budget, climate feedbacks and climate sensitivity (pp. 923–1054). https://doi.org/10.1017/9781009157896.009

Gong, S. L. (2003). A parameterization of sea-salt aerosol source function for sub- and super-micron particles. *Global Biogeochemical Cycles*, *17*(4). https://doi.org/10.1029/2003gb002079

Hardacre, C., Mulcahy, J. P., Pope, R. J., Jones, C. G., Rumbold, S. T., Li, C., et al. (2021). Evaluation of SO_2, SO_4^{2-} and an updated SO_2 dry deposition parameterization in the United Kingdom Earth System Model. *Atmospheric Chemistry and Physics*, *21*(24), 18465–18497. https://doi.org/10.5194/acp-21-18465-2021

Hersbach, H., Bell, B., Berrisford, P., Hirahara, S., Horányi, A., Muñoz-Sabater, J., et al. (2020). The ERA5 global reanalysis. *Quarterly Journal of the Royal Meteorological Society*, *146*(730), 1999–2049. https://doi.org/10.1002/qj.3803

Hodnebrog, Ø., Myhre, G., Jouan, C., Andrews, T., Forster, P. M., Jia, H., et al. (2024). Recent reductions in aerosol emissions have increased Earth's energy imbalance. *Communications Earth & Environment*, *5*(1), 166. https://doi.org/10.1038/s43247-024-01324-8

Hoesly, R. M., O'Rourke, P. R., Smith, S. J., Feng, L., Klimont, Z., Janssens-Maenhout, G., et al. (2020). CEDS v_2019_12_23 Emission Data (v_2019_12_23) [Dataset]. *Zenodo*. https://doi.org/10.5281/zenodo.3606753

Hoesly, R. M., Smith, S. J., Feng, L., Klimont, Z., Janssens-Maenhout, G., Pitkanen, T., et al. (2018). Historical (1750–2014) anthropogenic emissions of reactive gases and aerosols from the community emissions data system (CEDS). *Geoscientific Model Development*, *11*(1), 369–408. https://doi.org/10.5194/gmd-11-369-2018

Huang, J., Pan, X., Guo, X., Li, G., Li, G., Huang, J., et al. (2018). Health impact of China's air pollution prevention and control action plan: An analysis of national air quality monitoring and mortality data. *Articles Lancet Planet Health*, *2*(7), e313–e323. https://doi.org/10.1016/s2542-5196(18)30141-4

Huang, R. J., Zhang, Y., Bozzetti, C., Ho, K. F., Cao, J. J., Han, Y., et al. (2015). High secondary aerosol contribution to particulate pollution during haze events in China. *Nature*, *514*(7521), 218–222. https://doi.org/10.1038/nature13774

Ikeda, K., Tanimoto, H., Kanaya, Y., & Taketani, F. (2022). Evaluation of anthropogenic emissions of black carbon from East Asia in six inventories: Constraints from model simulations and surface observations on Fukue Island, Japan. *Environmental Science: Atmospheres*, *2*(3), 416–427. https://doi.org/10.1039/d1ea00051a

International Institute for Applied Systems Analysis (IIASA). (2019). ECLIPSE V6a global anthropogenic emissions [Dataset]. Retrieved from https://iiasa.ac.at/models-tools-data/global-emission-fields-of-air-pollutants-and-ghgs

IPCC. (2013). *Climate change 2013: The physical science basis: Summary for policymakers, a report of Working Group I of the IPCC, technical summary, a report accepted by Working Group I of the IPCC but not approved in detail and frequently asked questions: Part of the Working Group I contribution to the fifth assessment report of the Intergovernmental Panel on Climate Change*. Intergovernmental Panel on Climate Change.

Jin, Y., Andersson, H., & Zhang, S. (2016). Air pollution control policies in China: A retrospective and prospects. *International Journal of Environmental Research and Public Health*, *13*(12), 1219. MDPI. https://doi.org/10.3390/ijerph13121219

Johnson, B. T., & Haywood, J. M. (2023). Assessing the impact of self-lofting on increasing the altitude of black carbon in a global climate model. *Journal of Geophysical Research: Atmospheres*, *128*(8), e2022JD038039. https://doi.org/10.1029/2022JD038039

Johnson, B. T., Haywood, J. M., & Hawcroft, M. K. (2019). Are changes in atmospheric circulation important for black carbon aerosol impacts on clouds, precipitation, and radiation? *Journal of Geophysical Research: Atmospheres*, *124*(14), 7930–7950. https://doi.org/10.1029/2019JD030568

Kato, S., Rose, F. G., Rutan, D. A., Thorsen, T. J., Loeb, N. G., Doelling, D. R., et al. (2018). Surface irradiances of edition 4.0 clouds and the Earth's radiant energy system (CERES) energy balanced and filled (EBAF) data product. *Journal of Climate*, *31*(11), 4501–4527. https://doi.org/10.1175/JCLI-D-17-0523.1

Kelley, D. I., Bistinas, I., Whitley, R., Burton, C., Marthews, T. R., & Dong, N. (2019). How contemporary bioclimatic and human controls change global fire regimes. *Nature Climate Change*, *9*(9), 690–696. Nature Publishing Group. https://doi.org/10.1038/s41558-019-0540-7

Kirillina, K., Shvetsov, E. G., Protopopova, V. V., Thiesmeyer, L., & Yan, W. (2020). Consideration of anthropogenic factors in boreal forest fire regime changes during rapid socio-economic development: Case study of forestry districts with increasing burnt area in the Sakha Republic, Russia. *Environmental Research Letters*, *15*(3), 035009. https://doi.org/10.1088/1748-9326/ab6c6e

Leibensperger, E. M., Mickley, L. J., Jacob, D. J., Chen, W. T., Seinfeld, J. H., Nenes, A., et al. (2012). Climatic effects of 1950–2050 changes in US anthropogenic aerosols-Part 1: Aerosol trends and radiative forcing. *Atmospheric Chemistry and Physics*, *12*(7), 3333–3348. https://doi.org/10.5194/acp-12-3333-2012

Li, Z., Wang, Y., Guo, J., Zhao, C., Cribb, M. C., Dong, X., et al. (2019). East Asian study of tropospheric aerosols and their impact on regional clouds, precipitation, and climate (EAST-AIRCPC). *Journal of Geophysical Research: Atmospheres*, *124*(23), 13026–13054. Blackwell Publishing Ltd. https://doi.org/10.1029/2019JD030758

Liu, M., & Matsui, H. (2021). Aerosol radiative forcings induced by substantial changes in anthropogenic emissions in China from 2008 to 2016. *Atmospheric Chemistry and Physics*, *21*(8), 5965–5982. Copernicus GmbH. https://doi.org/10.5194/acp-21-5965-2021

Loeb, N. G., Doelling, D. R., Wang, H., Su, W., Nguyen, C., Corbett, J. G., et al. (2018). Clouds and the Earth's radiant energy system (CERES) energy balanced and filled (EBAF) top-of-atmosphere (TOA) edition-4.0 data product. *Journal of Climate*, *31*(2), 895–918. https://doi.org/10.1175/JCLI-D-17-0208.1

Mann, G. W., Carslaw, K. S., Spracklen, D. V., Ridley, D. A., Manktelow, P. T., Chipperfield, M. P., et al. (2010). Description and evaluation of GLOMAP-mode: A modal global aerosol microphysics model for the UKCA composition-climate model. *Geoscientific Model Development*, *3*(2), 519–551. https://doi.org/10.5194/gmd-3-519-2010

Mulcahy, J. P., Johnson, C., Jones, C. G., Povey, A. C., Scott, C. E., Sellar, A., et al. (2020). Description and evaluation of aerosol in UKESM1 and HadGEM3-GC3.1 CMIP6 historical simulations. *Geoscientific Model Development*, *13*(12), 6383–6423. https://doi.org/10.5194/gmd-13-6383-2020

Myhre, G., Aas, W., Cherian, R., Collins, W., Faluvegi, G., Flanner, M., et al. (2017). Multi-model simulations of aerosol and ozone radiative forcing due to anthropogenic emission changes during the period 1990–2015. *Atmospheric Chemistry and Physics*, *17*(4), 2709–2720. https://doi.org/10.5194/acp-17-2709-2017

Navarro, J. C. A., Varma, V., Riipinen, I., Seland, Kirkevåg, A., Struthers, H., et al. (2016). Amplification of Arctic warming by past air pollution reductions in Europe. *Nature Geoscience*, *9*(4), 277–281. https://doi.org/10.1038/ngeo2673

O'Connor, F. M., Johnson, C. E., Morgenstern, O., Abraham, N. L., Braesicke, P., Dalvi, M., et al. (2014). Evaluation of the new UKCA climate-composition model-Part 2: The troposphere. *Geoscientific Model Development*, *7*(1), 41–91. https://doi.org/10.5194/gmd-7-41-2014

O'Connor, F. M., Luke Abraham, N., Dalvi, M., Folberth, G. A., Griffiths, P. T., Hardacre, C., et al. (2021). Assessment of pre-industrial to present-day anthropogenic climate forcing in UKESM1. *Atmospheric Chemistry and Physics*, *21*(2), 1211–1243. https://doi.org/10.5194/acp-21-1211-2021

O'Rourke, P. R., Smith, S. J., Mott, A., Ahsan, H., McDuffie, E. E., Crippa, M., et al. (2021). *CEDS v_2021_04_21 release emission data*. Zenodo. https://doi.org/10.5281/zenodo.4741285

Pacifico, F., Folberth, G. A., Jones, C. D., Harrison, S. P., & Collins, W. J. (2012). Sensitivity of biogenic isoprene emissions to past, present, and future environmental conditions and implications for atmospheric chemistry. *Journal of Geophysical Research*, *117*(22). https://doi.org/10.1029/2012JD018276

Pacifico, F., Harrison, S. P., Jones, C. D., Arneth, A., Sitch, S., Weedon, G. P., et al. (2011). Evaluation of a photosynthesis-based biogenic isoprene emission scheme in JULES and simulation of isoprene emissions under present-day climate conditions. *Atmospheric Chemistry and Physics*, *11*(9), 4371–4389. https://doi.org/10.5194/acp-11-4371-2011

Petters, M. D., & Kreidenweis, S. M. (2007). A single parameter representation of hygroscopic growth and cloud condensation nucleus activity. *Atmospheric Chemistry and Physics*, *7*(8), 1961–1971. https://doi.org/10.5194/acp-7-1961-2007

Platnick, S., King, M., & Hubanks, P. (2017). MODIS atmosphere L3 monthly product. NASA MODIS Adaptive Processing System, Goddard Space Flight Center. https://doi.org/10.5067/MODIS/MYD08_M3.061

Quaas, J., Jia, H., Smith, C., Albright, A. L., Aas, W., Bellouin, N., et al. (2022). Robust evidence for reversal of the trend in aerosol effective climate forcing. *Atmospheric Chemistry and Physics*, *22*(18), 12221–12239. https://doi.org/10.5194/acp-22-12221-2022

Quinn, P. K., Shaw, G., Andrews, E., Dutton, E. G., Ruoho-Airola, T., & Gong, S. L. (2007). Arctic haze: Current trends and knowledge gaps. *Tellus Series B Chemical and Physical Meteorology*, *59*(1), 99–114. https://doi.org/10.1111/j.1600-0889.2006.00236.x

Randerson, J. T., van der Werf, G. R., Giglio, L., Collatz, G. J., & Kasibhatla, P. S. (2018). Global Fire Emissions Database, Version 4.1 (GFEDv4) [Dataset]. *ORNL DAAC, Oak Ridge, Tennessee, USA*. https://doi.org/10.3334/ORNLDAAC/1293

Rangel, M. A., & Vogl, T. S. (2019). Agricultural fires and health at birth. *The Review of Economics and Statistics*, *101*(4), 616–630. https://doi.org/10.1162/rest_a_00806

Rantanen, M., Karpechko, A. Y., Lipponen, A., Nordling, K., Hyvärinen, O., Ruosteenoja, K., et al. (2022). The Arctic has warmed nearly four times faster than the globe since 1979. *Communications Earth & Environment*, *3*(1), 168. https://doi.org/10.1038/s43247-022-00498-3

Samset, B. H., Wilcox, L. J., Allen, R. J., Stjern, C. W., Lund, M. T., Ahmadi, S., et al. (2025). East Asian aerosol cleanup has likely contributed to the recent acceleration in global warming. *Communications Earth & Environment*, *6*(1), 543. https://doi.org/10.1038/s43247-025-02527-3

Sand, M., Berntsen, T. K., Kay, J. E., Lamarque, J. F., Seland, & Kirkeväg, A. (2013). The Arctic response to remote and local forcing of black carbon. *Atmospheric Chemistry and Physics*, *13*(1), 211–224. https://doi.org/10.5194/acp-13-211-2013

Schacht, J., Heinold, B., Quaas, J., Backman, J., Cherian, R., Ehrlich, A., et al. (2019). The importance of the representation of air pollution emissions for the modeled distribution and radiative effects of black carbon in the Arctic. *Atmospheric Chemistry and Physics*, *19*(17), 11159–11183. https://doi.org/10.5194/acp-19-11159-2019

Schultz, M. G., Heil, A., Hoelzemann, J. J., Spessa, A., Thonicke, K., Goldammer, J. G., et al. (2008). Global wildland fire emissions from 1960 to 2000. *Global Biogeochemical Cycles*, *22*(2). https://doi.org/10.1029/2007GB003031

Sellar, A. A., Jones, C. G., Mulcahy, J. P., Tang, Y., Yool, A., Wiltshire, A., et al. (2019). UKESM1: Description and evaluation of the U.K. Earth system model. *Journal of Advances in Modeling Earth Systems*, *11*(12), 4513–4558. https://doi.org/10.1029/2019MS001739

Shindell, D., & Faluvegi, G. (2009). Climate response to regional radiative forcing during the twentieth century. *Nature Geoscience*, *2*(4), 294–300. https://doi.org/10.1038/ngeo473

Silver, B., Arnold, S. R., Reddington, C. L., Emmons, L. K., & Conibear, L. (2024). Large transboundary health impact of Arctic wildfire smoke. *Communications Earth & Environment*, *5*(1), 199. https://doi.org/10.1038/s43247-024-01361-3

Silver, B., Conibear, L., Reddington, C. L., Knote, C., Arnold, S. R., & Spracklen, D. V. (2020). Pollutant emission reductions deliver decreased $PM_{2.5}$-caused mortality across China during 2015–2017. *Atmospheric Chemistry and Physics*, *20*(20), 11683–11695. https://doi.org/10.5194/acp-20-11683-2020

Silver, B., Reddington, C. L., Arnold, S. R., & Spracklen, D. V. (2018). Substantial changes in air pollution across China during 2015–2017. *Environmental Research Letters*, *13*(11), 114012. https://doi.org/10.1088/1748-9326/aae718

Silver, B., Reddington, C. L., Chen, Y., & Arnold, S. R. (2025). A decade of China's air quality monitoring data suggests health impacts are no longer declining. *Environment International*, *197*, 109318. https://doi.org/10.1016/j.envint.2025.109318

Smith, S. J., & Mizrahi, A. (2013). Near-term climate mitigation by short-lived forcers. *Proceedings of the National Academy of Sciences of the United States of America*, *110*(35), 14202–14206. https://doi.org/10.1073/pnas.1308470110

Sobhani, N., Kulkarni, S., & Carmichael, G. R. (2018). Source sector and region contributions to black carbon and $PM_{2.5}$ in the Arctic. *Atmospheric Chemistry and Physics*, *18*(24), 18123–18148. https://doi.org/10.5194/acp-18-18123-2018

Stjern, C. W., Lund, M. T., Samset, B. H., Myhre, G., Forster, P. M., Andrews, T., et al. (2019). Arctic amplification response to individual climate drivers. *Journal of Geophysical Research: Atmospheres*, *124*(13), 6698–6717. https://doi.org/10.1029/2018JD029726

Stohl, A., Aamaas, B., Amann, M., Baker, L. H., Bellouin, N., Berntsen, T. K., et al. (2015). Evaluating the climate and air quality impacts of short-lived pollutants. *Atmospheric Chemistry and Physics*, *15*(18), 10529–10566. https://doi.org/10.5194/acp-15-10529-2015

Szopa, S., Naik, V., Adhikary, B., Artaxo, P., Berntsen, T., Collins, W. D., et al. (2021). Short-lived climate forcers. In *Climate change 2021—The physical science basis* (pp. 817–922). Cambridge University Press. https://doi.org/10.1017/9781009157896.008

Tian, C., Yue, X., Zhu, J., Liao, H., Yang, Y., Lei, Y., et al. (2022). Fire-climate interactions through the aerosol radiative effect in a global chemistry-climate-vegetation model. *Atmospheric Chemistry and Physics*, *22*(18), 12353–12366. https://doi.org/10.5194/acp-22-12353-2022

Turnock, S. T., Butt, E. W., Richardson, T. B., Mann, G. W., Reddington, C. L., Forster, P. M., et al. (2016). The impact of European legislative and technology measures to reduce air pollutants on air quality, human health and climate. *Environmental Research Letters*, *11*(2), 024010. https://doi.org/10.1088/1748-9326/11/2/024010

Turnock, S. T., Spracklen, D. V., Carslaw, K. S., Mann, G. W., Woodhouse, M. T., Forster, P. M., et al. (2015). Modelled and observed changes in aerosols and surface solar radiation over Europe between 1960 and 2009. *Atmospheric Chemistry and Physics*, *15*(16), 9477–9500. https://doi.org/10.5194/acp-15-9477-2015

von Salzen, K., Whaley, C. H., Anenberg, S. C., Van Dingenen, R., Klimont, Z., Flanner, M. G., et al. (2022). Clean air policies are key for successfully mitigating Arctic warming. *Communications Earth & Environment*, *3*(1), 222. https://doi.org/10.1038/s43247-022-00555-x

Voulgarakis, A., Marlier, M. E., Faluvegi, G., Shindell, D. T., Tsigaridis, K., & Mangeon, S. (2015). Interannual variability of tropospheric trace gases and aerosols: The role of biomass burning emissions. *Journal of Geophysical Research: Atmospheres*, *120*(14), 7157–7173. https://doi.org/10.1002/2014JD022926

Walters, D., Baran, A. J., Boutle, I., Brooks, M., Earnshaw, P., Edwards, J., et al. (2019). The met office unified model global atmosphere 7.0/7.1 and JULES Global Land 7.0 configurations. *Geoscientific Model Development*, *12*(5), 1909–1963. https://doi.org/10.5194/gmd-12-1909-2019

Wang, H., Zheng, X. T., Cai, W., Han, Z. W., Xie, S. P., Kang, S. M., et al. (2024). Atmosphere teleconnections from abatement of China aerosol emissions exacerbate Northeast Pacific warm blob events. *Proceedings of the National Academy of Sciences of the United States of America*, *121*(21), e2313797121. https://doi.org/10.1073/pnas.2313797121

Wang, Y., Zheng, X., Dong, X., Xi, B., Wu, P., Logan, T., & Yung, Y. L. (2020). Impacts of long-range transport of aerosols on marine-boundary-layer clouds in the eastern North Atlantic. *Atmospheric Chemistry and Physics*, *20*(23), 14741–14755. https://doi.org/10.5194/acp-20-14741-2020

Wang, Z., Lin, L., Xu, Y., Che, H., Zhang, X., Zhang, H., et al. (2021). Incorrect Asian aerosols affecting the attribution and projection of regional climate change in CMIP6 models. *npj Climate and Atmospheric Science*, *4*(1), 2. https://doi.org/10.1038/s41612-020-00159-2

Wasserman, T. N., & Mueller, S. E. (2023). Climate influences on future fire severity: A synthesis of climate-fire interactions and impacts on fire regimes, high-severity fire, and forests in the western United States. *Fire Ecology*, *19*(1), 43. Springer Science and Business Media Deutschland GmbH. https://doi.org/10.1186/s42408-023-00200-8

Wielicki, B. A., Barkstrom, B. R., Harrison, E. F., Lee, R. B., Smith, G. L., & Cooper, J. E. (1996). Clouds and the Earth's radiant energy system (CERES): An Earth observing system experiment.

Wilcox, L. J., Allen, R. J., Samset, B. H., Bollasina, M. A., Griffiths, P. T., Keeble, J., et al. (2023). The regional aerosol model intercomparison project (RAMIP). *Geoscientific Model Development*, *16*(15), 4451–4479. https://doi.org/10.5194/gmd-16-4451-2023

Williams, K. D., Copsey, D., Blockley, E. W., Bodas-Salcedo, A., Calvert, D., Comer, R., et al. (2018). The met office global coupled model 3.0 and 3.1 (GC3.0 and GC3.1) configurations. *Journal of Advances in Modeling Earth Systems*, *10*(2), 357–380. https://doi.org/10.1002/2017MS001115

Young, O. R., Guttman, D., Qi, Y., Bachus, K., Belis, D., Cheng, H., et al. (2015). Institutionalized governance processes. Comparing environmental problem solving in China and the United States. *Global Environmental Change*, *31*, 163–173. https://doi.org/10.1016/j.gloenvcha.2015.01.010

Yu, Y., Dai, C., Wei, Y., Ren, H., & Zhou, J. (2022). Air pollution prevention and control action plan substantially reduced $PM_{2.5}$ concentration in China. *Energy Economics*, *113*, 106206. https://doi.org/10.1016/j.eneco.2022.106206

Yue, H., He, C., Huang, Q., Yin, D., & Bryan, B. A. (2020). Stronger policy required to substantially reduce deaths from $PM_{2.5}$ pollution in China. *Nature Communications*, *11*(1), 1462. https://doi.org/10.1038/s41467-020-15319-4

Zhao, H., Gui, K., Yao, W., Shang, N., Zhang, X., Liang, Y., et al. (2024). Relative contributions of component-segregated aerosols to trends in aerosol optical depth over land (2007–2019): Insights from CAMS aerosol reanalysis. *Atmospheric Environment*, *333*, 120676. https://doi.org/10.1016/j.atmosenv.2024.120676

Zheng, B., Tong, D., Li, M., Liu, F., Hong, C., Geng, G., et al. (2018). Trends in China's anthropogenic emissions since 2010 as the consequence of clean air actions. *Atmospheric Chemistry and Physics*, *18*(19), 14095–14111. https://doi.org/10.5194/acp-18-14095-2018

Zheng, B., Zhang, Q., Geng, G., Chen, C., Shi, Q., Cui, M., et al. (2021). Changes in China's anthropogenic emissions and air quality during the COVID-19 pandemic in 2020. *Earth System Science Data*, *13*(6), 2895–2907. https://doi.org/10.5194/essd-13-2895-2021

Zheng, Y., Zhang, Q., Tong, D., Davis, S. J., & Caldeira, K. (2020). Climate effects of China's efforts to improve its air quality. *Environmental Research Letters*, *15*(10), 104052. https://doi.org/10.1088/1748-9326/ab9e21

Zhu, Q., Liu, Y., Shao, T., & Tang, Y. (2020). Transport of Asian aerosols to the Pacific Ocean. *Atmospheric Research*, *234*, 104735. https://doi.org/10.1016/j.atmosres.2019.104735